Buckling and Post-Buckling of Thin Elastoplastic Cylindrical Shells With Finite Rotations

Philippe Le Grognec, Anh Le Van

BUCKLING AND POST-BUCKLING OF THIN ELASTOPLASTIC CYLINDRICAL SHELLS WITH FINITE ROTATIONS

Philippe Le Grognec
Ecole Centrale de Nantes
Laboratoire de Mécanique et Matériaux
Division Structures
1, rue de la Noë BP 92101
44321 Nantes Cedex 3 France
E-mail : Philippe.Le-Grognec@ec-nantes.fr

Anh Le Van
Ecole Centrale de Nantes
Laboratoire de Mécanique et Matériaux
Division Structures
1, rue de la Noë BP 92101
44321 Nantes Cedex 3 France
E-mail : Anh.Le-Van@ec-nantes.fr

ABSTRACT

An elastoplastic thin shell model is presented in this work in order to compute the buckling and post-buckling behavior of cylindrical shell-type structures. Standard assumptions in the shell kinematics allow us to develop a large deformation and finite rotation model for thin shells from the three-dimensional continuum.

An elastoplastic constitutive model for thin shells is derived from the three-dimensional framework, assuming the plane stress condition. The von Mises yield criterion is adopted including non-linear isotropic and linear kinematic hardening.

The resulting non-linear system is solved by a Newton-Raphson solution procedure, including the consistent linearization of the shell kinematics and the elastoplastic material model.

The high non-linearities due to the buckling-type instabilities, especially those occuring in the neighbourhood of critical points, necessitate the use of an appropriate step-length control. An arc-length method has been successfully implemented for passing through limit points (load or displacement peaks) where pure load or displacement controls fail. The proposed method is effective in handling both sharp snap-throughs and snap-backs.

Two numerical examples are presented in view of the assessment of the proposed approach and a particular attention is devoted to the post-buckling of hollow cylinders under axial compression. We identify several types of buckling mode for these structures, among which the axisymmetric mode, the "diamond" mode and the "elephant foot" mode, depending on geometry and boundary conditions.

NOMENCLATURE

- $\vec{P}_0$ Position vector of a particle on the middle surface at the reference configuration
- $\vec{P}_t$ Position vector of a particle on the middle surface at the deformed configuration
- $\vec{T}$ Director field at the reference configuration
- $\vec{t}$ Director field at the deformed configuration
- $\vec{X}$ Position vector of a particle in the shell body at the reference configuration
- $\vec{x}$ Position vector of a particle in the shell body at the deformed configuration
- ξ, η Local surface co-ordinates
- ζ Local through-thickness co-ordinate
- Ω Shell volume
- $\mathcal{M}$ Shell middle surface
- $\otimes$ Tensor product
  Contracted products

INTRODUCTION

Buckling and post-buckling phenomena involve both geometric and material non-linearities. An elastoplastic thin shell

model with finite strains and finite rotations is presented in this work in order to compute the response of hollow structures under such conditions of compressive loading. A total Lagrangian formulation is employed.

The originally strain driven return mapping algorithm has been transformed in order to include the plane stress condition in the plastic correction (Simo and Taylor, 1986).

The finite element formulation is based on eight-node isoparametric shell elements. The introduction of general elastoplastic constitutive laws makes it necessary to use numerical integration through the shell thickness in order to compute the stress resultant tensors and their derivatives. Numerical results may then be compared with those obtained using the stress resultant model of Simo and Kennedy (1992).

A robust arc-length method has finally been implemented with an appropriate step control to systematically pass through all sorts of limit points.

The "elephant foot" transition mode, occuring in a secondary bifurcation path, as shown in the results below, especially show the high performance of the formulation in simulating buckling and post-buckling phenomena.

1 ELASTOPLASTIC THIN SHELL MODEL

1.1 Shell kinematics

1.1.1 Preliminaries In the present work, the shell-like body is represented by a middle surface and an independent director field in the thickness direction of the shell. The director field is not constrained to be normal to the middle surface, except at the reference configuration (Mindlin-Reissner type formulation).

The reference and deformed configurations may be represented respectively as :

$$\begin{aligned} \vec{X} &= \vec{P}_0(\xi,\eta) + \zeta\vec{T}(\xi,\eta) \\ \vec{x} &= \vec{P}_t(\xi,\eta) + \zeta\vec{t}(\xi,\eta) \end{aligned} \tag{1}$$

The displacement at a point $\vec{X}(\xi,\eta,\zeta)$ can be written as :

$$\vec{D}(\xi,\eta,\zeta) = \vec{U}(\xi,\eta) + \zeta(\vec{t}(\xi,\eta) - \vec{T}(\xi,\eta)) \tag{2}$$

where $\vec{U}(\xi,\eta) = \vec{P}_t(\xi,\eta) - \vec{P}_0(\xi,\eta)$ is the displacement of the corresponding middle surface point.

All vectors will be written in a Cartesian basis :

$$\vec{X} = X^i\vec{e}_i,\ \vec{T} = T^i\vec{e}_i,\ \vec{x} = x^i\vec{e}_i,\ \vec{t} = t^i\vec{e}_i \tag{3}$$

where implicit summations are made on repeated indices.

1.1.2 The deformation gradient The deformation gradient may be written as :

$$\bar{\bar{F}} = \vec{g}_i \otimes \vec{G}^i \tag{4}$$

where :

$$\begin{aligned} \vec{G}_1 &= \frac{\partial\vec{X}}{\partial\xi},\ \vec{G}_2 = \frac{\partial\vec{X}}{\partial\eta},\ \vec{G}_3 = \frac{\partial\vec{X}}{\partial\zeta} \\ \vec{g}_1 &= \frac{\partial\vec{x}}{\partial\xi},\ \vec{g}_2 = \frac{\partial\vec{x}}{\partial\eta},\ \vec{g}_3 = \frac{\partial\vec{x}}{\partial\zeta} \end{aligned} \tag{5}$$

define the local covariant bases in the reference and actual configurations and $\{\vec{G}^i\}_{i=1,2,3}$ is the contravariant basis dual to $\{\vec{G}_i\}_{i=1,2,3}$.

These bases $\{\vec{G}_i\}_{i=1,2,3}$ and $\{\vec{G}^i\}_{i=1,2,3}$ will further be replaced by $\{\vec{A}_i\}_{i=1,2,3}$ and $\{\vec{A}^i\}_{i=1,2,3}$ defined on the middle surface, neglecting the variation of the metric through the shell thickness. Therefore, the metric tensor may be defined respectively in its covariant and contravariant components as $A_{ij} = \vec{A}_i.\vec{A}_j$ and $A^{ij} = \vec{A}^i.\vec{A}^j$.

It follows from the definition of $\bar{\bar{F}}$ and Eq.(5) :

$$\bar{\bar{F}} = (\vec{a}_\alpha \otimes \vec{A}^\alpha + \vec{t} \otimes \vec{T}) + \vec{t}_{,\alpha} \otimes \vec{A}^\alpha \tag{6}$$

where Greek indices take the values 1 or 2.

1.1.3 Finite rotation operator The motion of the inextensible director is given by :

$$\vec{t} = \bar{\bar{R}}.\vec{T} \tag{7}$$

where the finite rotation tensor $\bar{\bar{R}}$ is orthogonal ($\bar{\bar{R}}^{-1} = \bar{\bar{R}}^T$ and $det\ \bar{\bar{R}} = 1$) and can be associated with the skew-symmetric tensor $\bar{\bar{\Theta}}$ by the exponential mapping :

$$\bar{\bar{R}} = exp\ \bar{\bar{\Theta}} = \sum_{k=0}^{+\infty} \frac{\bar{\bar{\Theta}}^k}{k!} \tag{8}$$

Then the axial vector $\vec{\theta}$ may be defined such that $\bar{\bar{\Theta}}.\vec{\theta} = \vec{0}$ and $\bar{\bar{\Theta}}.\vec{v} = \vec{\theta} \wedge \vec{v},\ \forall\vec{v} \in \mathbb{R}^3$. From the relation $\bar{\bar{R}}.\vec{\theta} = \vec{\theta}$, it clearly follows that $\bar{\bar{R}}$ defines the rotation about $\vec{\theta}$.

Equivalently, the Rodrigues formula leads to an explicit form of Eq.(8) :

$$\bar{\bar{R}} = \cos\theta \bar{\bar{I}} + \frac{\sin\theta}{\theta}\bar{\bar{\Theta}} + \frac{1-\cos\theta}{\theta^2}\vec{\theta}\otimes\vec{\theta} \tag{9}$$

where $\theta = ||\vec{\theta}||$ defines the magnitude of the rotation.

Since $\vec{\theta}$ is perpendicular to $\vec{T}$ and, therefore, to $\vec{t}$, the director field $\vec{t}$ may then be written in the simplified following form :

$$\vec{t} = \bar{\bar{R}}.\vec{T} = \cos\theta\vec{T} + \frac{\sin\theta}{\theta}\vec{\theta}\wedge\vec{T} \tag{10}$$

In the Cartesian fixed basis $\{\vec{e}_i\}_{i=1,2,3}$, with $\vec{\theta} = \theta^i\vec{e}_i$:

$$\begin{Bmatrix} t^1 \\ t^2 \\ t^3 \end{Bmatrix} = \cos\theta \begin{Bmatrix} T^1 \\ T^2 \\ T^3 \end{Bmatrix} + \frac{\sin\theta}{\theta} \begin{Bmatrix} \theta^2T^3 - \theta^3T^2 \\ \theta^3T^1 - \theta^1T^3 \\ \theta^1T^2 - \theta^2T^1 \end{Bmatrix} \tag{11}$$

By using a new local orthonormal basis $\{\vec{E}_i\}_{i=1,2,3}$ at each point of the middle surface : $\vec{E}_3 = \vec{T}$, $\vec{E}_1 = \frac{\vec{A}_1}{\|\vec{A}_1\|}$ and $\vec{E}_2 = \vec{E}_3\wedge\vec{E}_1$, with $\vec{\theta} = \hat{\theta}^1\vec{E}_1 + \hat{\theta}^2\vec{E}_2$, Eq.(11) can be recast as :

$$\begin{Bmatrix} \hat{t}^1 \\ \hat{t}^2 \\ \hat{t}^3 \end{Bmatrix} = \cos\theta \begin{Bmatrix} 0 \\ 0 \\ 1 \end{Bmatrix} + \frac{\sin\theta}{\theta} \begin{Bmatrix} \hat{\theta}^2 \\ -\hat{\theta}^1 \\ 0 \end{Bmatrix} \tag{12}$$

1.1.4 Variations of kinematic variables The linearization of kinematic variables at a given configuration is performed by a systematic use of the directional derivative to a one-parameter family of configurations. Thus, all the variations and incremental quantities are obtained by an ordinary differentiation with respect to the small parameter ε.

The following relations hold in the vicinity of $\varepsilon = 0$:

$$\begin{aligned} \vec{P}_\varepsilon &= \vec{P} + \varepsilon\delta\vec{U} \\ \vec{t}_\varepsilon &= \bar{\bar{R}}_\varepsilon.\vec{T} = \bar{\bar{R}}(\vec{\theta} + \varepsilon\delta\vec{\theta}).\vec{T} \end{aligned} \tag{13}$$

which yield :

$$(\delta\vec{P}, \delta\vec{t}) = \frac{d}{d\varepsilon}|_{\varepsilon=0}(\vec{P}_\varepsilon, \vec{t}_\varepsilon) \tag{14}$$

and :

$$\begin{aligned} \delta\vec{P} &= \delta\vec{U} \\ \delta\vec{t} &= \tfrac{\sin\theta}{\theta}[-(\vec{\theta}.\delta\vec{\theta})\vec{T} + \delta\vec{\theta}\wedge\vec{T}] \\ &\quad + \tfrac{\theta\cos\theta - \sin\theta}{\theta^3}(\vec{\theta}.\delta\vec{\theta})(\vec{\theta}\wedge\vec{T}) \end{aligned} \tag{15}$$

The latter relation can be written in the local basis :

$$\begin{Bmatrix} \delta\hat{t}^1 \\ \delta\hat{t}^2 \\ \delta\hat{t}^3 \end{Bmatrix} = [\Phi] \begin{Bmatrix} \delta\hat{\theta}^1 \\ \delta\hat{\theta}^2 \end{Bmatrix}$$

$$[\Phi] = \left[-\tfrac{\sin\theta}{\theta} \begin{bmatrix} 0 & -1 \\ 1 & 0 \\ \hat{\theta}^1 & \hat{\theta}^2 \end{bmatrix} + \tfrac{\sin\theta - \theta\cos\theta}{\theta^3} \begin{bmatrix} -\hat{\theta}^2\hat{\theta}^1 & -\hat{\theta}^2\hat{\theta}^2 \\ \hat{\theta}^1\hat{\theta}^1 & \hat{\theta}^1\hat{\theta}^2 \\ 0 & 0 \end{bmatrix} \right] \tag{16}$$

and then transformed in the standard basis for computational purposes.

1.2 Elastoplastic constitutive material model

1.2.1 Strain measures The Green strain tensor $\bar{\bar{E}}$ is given by the relation :

$$\bar{\bar{E}} = \frac{1}{2}(\bar{\bar{F}}^T.\bar{\bar{F}} - \bar{\bar{I}}) \tag{17}$$

Using its components relative to the contravariant basis $\{\vec{A}^i\}_{i=1,2,3}$:

$$\bar{\bar{E}} = \frac{1}{2}(\vec{a}_i.\vec{a}_j - \vec{A}_i.\vec{A}_j)\vec{A}^i\otimes\vec{A}^j = E_{ij}\vec{A}^i\otimes\vec{A}^j \tag{18}$$

or :

$$\bar{\bar{E}} = E_{\alpha\beta}\vec{A}^\alpha\otimes\vec{A}^\beta + E_{\alpha 3}\vec{A}^\alpha\otimes\vec{T} + E_{3\alpha}\vec{T}\otimes\vec{A}^\alpha + E_{33}\vec{T}\otimes\vec{T} \tag{19}$$

These components of $\bar{\bar{E}}$ may be written as functions of the through-thickness parameter ζ :

$$E_{ij} = E_{ij}^{(0)} + \zeta E_{ij}^{(1)} + \zeta^2 E_{ij}^{(2)} \tag{20}$$

where, decomposing $\vec{a}_\alpha$ into $\vec{a}_\alpha = \vec{A}_\alpha + \vec{U}_{,\alpha}$:

$$
\begin{aligned}
E^{(0)}_{\alpha\beta} &= \tfrac{1}{2}(\vec{A}_\alpha.\vec{U}_{,\beta} + \vec{A}_\beta.\vec{U}_{,\alpha} + \vec{U}_{,\alpha}.\vec{U}_{,\beta}) \\
E^{(0)}_{\alpha 3} &= E^{(0)}_{3\alpha} = \tfrac{1}{2}(\vec{A}_\alpha.(\vec{t} - \vec{T}) + \vec{U}_{,\alpha}.\vec{t}) \\
E^{(1)}_{\alpha\beta} &= \tfrac{1}{2}(\vec{A}_\alpha.(\vec{t}_{,\beta} - \vec{T}_{,\beta}) + \vec{A}_\beta.(\vec{t}_{,\alpha} - \vec{T}_{,\alpha}) \\
&\quad + \vec{U}_{,\alpha}.\vec{t}_{,\beta} + \vec{U}_{,\beta}.\vec{t}_{,\alpha}) \\
E^{(2)}_{\alpha\beta} &= \tfrac{1}{2}(\vec{t}_{,\alpha}.\vec{t}_{,\beta} - \vec{T}_{,\alpha}.\vec{T}_{,\beta})
\end{aligned}
\tag{21}
$$

All other components, in particular $E^{(0)}_{33}$, $E^{(1)}_{33}$ and $E^{(2)}_{33}$, are zero since the director field is assumed to be inextensible (see Eq.(7)). However, the value of E_{33} can be directly derived by applying the plane stress condition.

Variations of these quantities can then be computed by :

$$
\delta\bar{\bar{E}} = \frac{d}{d\varepsilon}|_{\varepsilon=0}\bar{\bar{E}}(\vec{P}_\varepsilon, \vec{t}_\varepsilon) \tag{22}
$$

namely :

$$
\begin{aligned}
\delta E^{(0)}_{\alpha\beta} &= \tfrac{1}{2}((\vec{A}_\alpha + \vec{U}_{,\alpha}).\delta\vec{U}_{,\beta} + (\vec{A}_\beta + \vec{U}_{,\beta}).\delta\vec{U}_{,\alpha}) \\
\delta E^{(0)}_{\alpha 3} &= \delta E^{(0)}_{3\alpha} = \tfrac{1}{2}((\vec{A}_\alpha + \vec{U}_{,\alpha}).\delta\vec{t} + \delta\vec{U}_{,\alpha}.\vec{t}) \\
\delta E^{(1)}_{\alpha\beta} &= \tfrac{1}{2}((\vec{A}_\alpha + \vec{U}_{,\alpha}).\delta\vec{t}_{,\beta} + (\vec{A}_\beta + \vec{U}_{,\beta}).\delta\vec{t}_{,\alpha} \\
&\quad + \delta\vec{U}_{,\alpha}.\vec{t}_{,\beta} + \delta\vec{U}_{,\beta}.\vec{t}_{,\alpha}) \\
\delta E^{(2)}_{\alpha\beta} &= \tfrac{1}{2}(\delta\vec{t}_{,\alpha}.\vec{t}_{,\beta} + \vec{t}_{,\alpha}.\delta\vec{t}_{,\beta})
\end{aligned}
\tag{23}
$$

1.2.2 Stress tensor The second Piola-Kirchhoff stress tensor may be defined in the basis $\{\vec{A}_i\}_{i=1,2,3}$ as :

$$
\bar{\bar{\Sigma}} = \Sigma^{ij}\vec{A}_i \otimes \vec{A}_j \tag{24}
$$

or :

$$
\bar{\bar{\Sigma}} = \Sigma^{\alpha\beta}\vec{A}_\alpha \otimes \vec{A}_\beta + \Sigma^{\alpha 3}\vec{A}_\alpha \otimes \vec{T} + \Sigma^{3\alpha}\vec{T} \otimes \vec{A}_\alpha + \Sigma^{33}\vec{T} \otimes \vec{T} \tag{25}
$$

Then, three stress resultant tensors can be expressed as :

$$
\begin{aligned}
\bar{\bar{n}} &= n^{ij}\vec{A}_i \otimes \vec{A}_j \qquad n^{ij} = \int_{-\frac{h}{2}}^{\frac{h}{2}} \Sigma^{ij} d\zeta \\
\bar{\bar{m}}^{(1)} &= m^{ij(1)}\vec{A}_i \otimes \vec{A}_j \qquad m^{ij(1)} = \int_{-\frac{h}{2}}^{\frac{h}{2}} \Sigma^{ij}\zeta d\zeta \\
\bar{\bar{m}}^{(2)} &= m^{ij(2)}\vec{A}_i \otimes \vec{A}_j \qquad m^{ij(2)} = \int_{-\frac{h}{2}}^{\frac{h}{2}} \Sigma^{ij}\zeta^2 d\zeta
\end{aligned}
\tag{26}
$$

1.2.3 Hyperelastic model The three-dimensional St-Venant-Kirchhoff law is used in order to describe the hyperelastic response of the structure :

$$
\bar{\bar{\Sigma}} = \lambda(tr\bar{\bar{E}})\bar{\bar{I}} + 2\mu\bar{\bar{E}} = \bar{\bar{\bar{\bar{H}}}} : \bar{\bar{E}} \tag{27}
$$

with the Lamé parameters expressed as :

$$
\lambda = \frac{E\nu}{(1+\nu)(1-2\nu)}, \qquad \mu = \frac{E}{2(1+\nu)} \tag{28}
$$

One can express the constitutive law in the covariant and contravariant bases :

$$
\Sigma^{ij} = H^{ijkl}E_{lk} = (\lambda A^{ij}A^{kl} + \mu(A^{ik}A^{jl} + A^{il}A^{jk}))E_{lk} \tag{29}
$$

Enforcing the plane stress condition $\Sigma^{33} = 0$ in Eq.(29) leads to the shell hyperelastic model and the reduced fourth-order tensor :

$$
C^{ijkl} = H^{ijkl} - \frac{H^{33kl}}{H^{3333}}H^{ij33} \qquad ij \neq 33,\ kl \neq 33 \tag{30}
$$

and then :

$$
\begin{aligned}
n^{ij} &= \int_{-\frac{h}{2}}^{\frac{h}{2}} C^{ijkl}(E^{(0)}_{lk} + \zeta E^{(1)}_{lk} + \zeta^2 E^{(2)}_{lk})d\zeta \\
m^{ij(1)} &= \int_{-\frac{h}{2}}^{\frac{h}{2}} C^{ijkl}(E^{(0)}_{lk} + \zeta E^{(1)}_{lk} + \zeta^2 E^{(2)}_{lk})\zeta d\zeta \\
m^{ij(2)} &= \int_{-\frac{h}{2}}^{\frac{h}{2}} C^{ijkl}(E^{(0)}_{lk} + \zeta E^{(1)}_{lk} + \zeta^2 E^{(2)}_{lk})\zeta^2 d\zeta
\end{aligned}
\tag{31}
$$

According to the thin shell assumptions, the strain components $E^{(2)}_{ij}$ will further be neglected.

1.2.4 Elastoplastic model The strain tensor is additively decomposed into its elastic and plastic parts :

$$\bar{\bar{E}} = \bar{\bar{E}}^e + \bar{\bar{E}}^p \tag{32}$$

The yield criterion is of the von Mises type with a combination of non-linear isotropic and linear kinematic hardening :

$$f = \frac{1}{2}(\bar{\bar{S}} - \bar{\bar{\alpha}}') : (\bar{\bar{S}} - \bar{\bar{\alpha}}') - \frac{1}{3}(\sigma_0 + K(p))^2 \tag{33}$$

where $\bar{\bar{S}}$ represents the deviatoric part of the stress tensor $\bar{\bar{\Sigma}}$ and $\bar{\bar{\alpha}}'$ the back stress tensor caracterizing the kinematic hardening ($\alpha'_{kk} = 0$). Finally, the scalar p defines the equivalent plastic strain and $K(p)$ the isotropic hardening function.

For computational purposes, all equations will further be written in matrix notation. However, vectors and matrices are always expressed in covariant or contravariant basis.

The previous criterion can then be written as :

$$f = \frac{1}{2}\eta^T P \eta - \frac{1}{3}(\sigma_0 + K(p))^2 \tag{34}$$

where P is a deviatoric operator, $\eta = \Sigma - \alpha$ and α is defined such as $\alpha' = P\alpha$ and $\alpha^{33} = 0$.

The plastic flow and hardening rules read :

$$\begin{aligned} \dot{E}^p &= \dot{\lambda} P \eta \\ \dot{\alpha} &= \tfrac{2}{3} H \dot{\lambda} \eta \\ \dot{p} &= \dot{\lambda}\sqrt{\tfrac{2}{3}\eta^T P \eta} \end{aligned} \tag{35}$$

where H is the kinematic hardening parameter and $\dot{\lambda}$ the so-called consistency parameter.

A radial return algorithm is proposed in this work to describe the elastoplastic material behavior. The return mapping algorithms have always been strain driven and satisfaction of the plane stress condition places, especially here, a non-trivial constraint on the return algorithm.

The implicit Euler scheme is employed as the numerical time integration procedure. Assuming the displacement vector and hence the strain E_{n+1} are given at time t_{n+1}, the problem consists in estimating the stress Σ_{n+1}, the internal variables E^p_{n+1} and p_{n+1} at the same time instant t_{n+1}.

Use is made of a consistent elastoplastic tangent modulus in order to compute the structural tangent stiffness matrix.

The general procedure is summed up in the following elastic predictor - plastic corrector algorithm :

(i) Evaluate elastic predictor :

$$\begin{aligned} \Sigma^E &= C(E_{n+1} - E^p_n) \\ \eta^E &= \Sigma^E - \alpha_n \\ p^E &= p_n \end{aligned}$$

where C represents the matrix notation of tensor $\bar{\bar{\bar{\bar{C}}}}$.

(ii) Evaluate f using η^E and p^E :

If f negative :

$$\begin{aligned} \Sigma_{n+1} &= \Sigma^E \\ \eta_{n+1} &= \eta^E \\ p_{n+1} &= p^E = p_n \\ \alpha_{n+1} &= \alpha_n \\ E^p_{n+1} &= E^p_n \\ C^p_{n+1} &= \frac{\partial \Sigma_{n+1}}{\partial E_{n+1}} = C \end{aligned}$$

otherwise, evaluate the consistency parameter λ (λ stands for $\Delta\lambda$) by a Newton-Raphson iterative procedure, by solving :

$$f = \frac{1}{2}\eta^T_{n+1} P \eta_{n+1} - \frac{1}{3}(\sigma_0 + K(p_{n+1}))^2 = 0$$

with :

$$\eta_{n+1} = \frac{1}{1+\frac{2}{3}\lambda H}\Gamma(\lambda) C^{-1} \eta^E \qquad (\Gamma(\lambda) = (C^{-1} + \frac{\lambda}{1+\frac{2}{3}\lambda H} P)^{-1})$$

$$p_{n+1} = p_n + \lambda\sqrt{\tfrac{2}{3}\eta^T_{n+1} P \eta_{n+1}}$$

and update the other quantities :

$$\alpha_{n+1} = \alpha_n + \frac{2}{3}\lambda H \eta_{n+1}$$

$$\Sigma_{n+1} = \eta_{n+1} - \alpha_{n+1}$$

$$E^p_{n+1} = E^p_n + \lambda P \eta_{n+1}$$

$$C^p_{n+1} = \frac{\partial \Sigma_{n+1}}{\partial E_{n+1}} = \Gamma(\lambda) - \frac{(\Gamma(\lambda)P\eta_{n+1})(\Gamma(\lambda)P\eta_{n+1})^T}{\eta^T_{n+1}P^T\Gamma(\lambda)P\eta_{n+1}+\mu}$$

with :

$$\mu = \frac{2}{3}\frac{\gamma_1}{\gamma_2}(K'(p_{n+1})\gamma_1 + H\gamma_2)\eta^T_{n+1}P\eta_{n+1}$$

$$(\gamma_1 = 1 + \frac{2}{3}\lambda H,\ \gamma_2 = 1 - \frac{2}{3}\lambda K'(p_{n+1}))$$

1.2.5 Weak formulation The principle of virtual work reads :

$$\mathcal{T} = \mathcal{T}_{int} + \mathcal{T}_{ext} = 0 \tag{36}$$

with :

$$\mathcal{T}_{int} = -\int_\Omega \bar{\bar{\Sigma}} : \delta\bar{\bar{E}} dV \tag{37}$$

and :

$$\begin{aligned}\mathcal{T}_{ext} = &\int_\Omega \vec{f}^p.\delta\vec{P}dV + \int_\Omega \vec{f}^t.\delta\vec{t}dV \\ &+ \int_{\partial\Omega}\vec{\tau}^p.\delta\vec{P}dS + \int_{\partial\Omega}\vec{\tau}^t.\delta\vec{t}dS\end{aligned} \tag{38}$$

More precisely, the internal virtual work may be expressed as :

$$\mathcal{T}_{int} = -\int_{\mathcal{M}}\left(\int_{-\frac{h}{2}}^{\frac{h}{2}} \Sigma^{ij}(\delta E^{(0)}_{ji} + \zeta\delta E^{(1)}_{ji})d\zeta\right)dA \tag{39}$$

which results in :

$$-\int_{\mathcal{M}}(n^{ij}\delta E^{(0)}_{ji} + m^{ij(1)}\delta E^{(1)}_{ji})dA + \mathcal{T}_{ext} = 0 \tag{40}$$

2 NUMERICAL IMPLEMENTATION

2.1 Finite element formulation

2.1.1 Interpolation The geometry of the middle surface and the associated displacements are described by an eight-node isoparametric shell finite element, with classical bi-linear shape functions. The director fields $\vec{T}$ and $\vec{t}$ are interpolated in the same way.

Attention should be drawn on two types of discretization errors :

- The interpolation of $\vec{P}_0$ leads to several normals (one for each adjoined element) at each node.
- The interpolated $\vec{T}$ does not coincide with the normal at the surface defined by the interpolation of $\vec{P}_0$.

All the previous fields can be expressed, with $\mathcal{N} = 8$, as :

$$\begin{aligned}\vec{P}_0(\xi,\eta) &= \textstyle\sum_{i=1}^{\mathcal{N}} N^i(\xi,\eta)\vec{P}_{0i} \\ \vec{T}(\xi,\eta) &= \textstyle\sum_{i=1}^{\mathcal{N}} N^i(\xi,\eta)\vec{T}_i \\ \vec{U} &= \textstyle\sum_{i=1}^{\mathcal{N}} N^i(\xi,\eta)\vec{U}_i \\ \vec{t} &= \textstyle\sum_{i=1}^{\mathcal{N}} N^i(\xi,\eta)\vec{t}_i\end{aligned} \tag{41}$$

The following variations and derivatives of these fields will be required :

$$\begin{aligned}\vec{U}_{,\alpha} &= \textstyle\sum_{i=1}^{\mathcal{N}} N^i_{,\alpha}\vec{U}_i \\ \delta\vec{U}_{,\alpha} &= \textstyle\sum_{i=1}^{\mathcal{N}} N^i_{,\alpha}\delta\vec{U}_i \\ \vec{t}_{,\alpha} &= \textstyle\sum_{i=1}^{\mathcal{N}} N^i_{,\alpha}\vec{t}_i \\ \delta\vec{t} &= \textstyle\sum_{i=1}^{\mathcal{N}} N^i\delta\vec{t}_i \\ \delta\vec{t}_{,\alpha} &= \textstyle\sum_{i=1}^{\mathcal{N}} N^i_{,\alpha}\delta\vec{t}_i\end{aligned} \tag{42}$$

The second derivatives will also be required :

$$\begin{aligned}\Delta(\delta\vec{t}) &= \textstyle\sum_{i=1}^{\mathcal{N}} N^i\Delta(\delta\vec{t}_i) \\ \Delta(\delta\vec{t}_{,\alpha}) &= \textstyle\sum_{i=1}^{\mathcal{N}} N^i_{,\alpha}\Delta(\delta\vec{t}_i)\end{aligned} \tag{43}$$

Eventually, there are five degrees of freedom at each node. three translations and two rotations in the tangent space.

2.1.2 Numerical integration The Gaussian points are equally distributed in the reference square element in order to compute surface integrals and are also needed through the shell thickness.

At each Gaussian point of the middle surface, the real tangent vectors are computed by the interpolation of $\vec{P}_0$:

$$\vec{A}_1 = \vec{P}_{0,1} = \sum_{i=1}^{\mathcal{N}} N^i_{,1} \vec{P}_{0i}$$
$$\vec{A}_2 = \vec{P}_{0,2} = \sum_{i=1}^{\mathcal{N}} N^i_{,2} \vec{P}_{0i} \tag{44}$$

so that the reference square element can relate to the real one.

2.1.3 Newton-Raphson solution procedure All variables are expressed in standard matrix notation, separating membrane, shear and bending terms. The internal and external force vectors, issued from the equivalent virtual works, are naturally computed by assembling element quantities.

Denoting $\mathcal{T}_{ext} = \{\delta\mathcal{U}\}^T\{F\}$ and $\mathcal{T}_{int} = -\{\delta\mathcal{U}\}^T\{\psi\}$, Eq.(40) is now replaced by :

$$\{\delta\mathcal{U}\}^T(\{\psi\} - \{F\}) = 0 \tag{45}$$

The non-linear system $\{\psi(\mathcal{U})\} = \{F\}$ is solved by an iterative Newton-Raphson procedure. The most important step of the procedure is the linearization of the whole system (including geometric and material non-linearities), which consists in the construction of the tangent stiffness matrix :

$$[K_T] = \frac{\partial\{\psi(\mathcal{U})\}}{\partial\{\mathcal{U}\}} \tag{46}$$

The computation of the geometric part of $[K_T]$ necessitates the estimation of $\Delta(\delta\vec{t}_i)$ at the middle surface nodes. It demands a more complicated but similar development. The interested reader is referred to Brank *et al.* (1997) for details.

It should be noted that $\Delta(\delta\vec{U})$ is always zero.

Finally, it is necessary to define a local orthonormal basis at each node in correspondence with the Cartesian fixed basis in order to describe $\vec{\theta}$ in every adjoined element in a coherent way.

2.2 Arc-length method

It is important to be able to proceed beyond limit points resulting from the non-linearities due to material behavior and large geometry change especially encountered in buckling phenomena.

Load control methods naturally present difficulties near load peaks. Displacement control, which treats the load intensity as unknown, can only handle snap-throughs (but not snap-backs) and the choice of pattern for the displacement to be controlled is not easy.

Arc-length methods are more satisfactory in that they systematically pass through all sorts of peaks.

A new solution procedure, based on the arc-length method (Crisfield, 1981), is presented in this section. It especially proposes various means for avoiding complex roots in the quadratic constraint equation (Lam and Morley, 1995).

In this section, U and F represent nodal displacement and load vectors, respectively.

2.2.1 Quadratic arc-length method Crisfield (1981) has successfully applied a modified arc-length method from the constant arc-length method of Riks and Wempner.

The constraint equation :

$$D = \Delta U^T \Delta U + \Delta\lambda^2 \psi^2 F^T F - \Delta l^2 = 0 \tag{47}$$

where ΔU is the trial incremental displacement vector, $\Delta\lambda$ the incremental load factor, F the reference external load vector, Δl the specified arc-length and ψ a scaling parameter, was originally solved simultaneously with the equilibrium equations. The symmetric banded nature of the stiffness matrix was automatically lost.

The idea was to write, at the i-th iteration :

$$\delta U_i = \delta U_{iR} + \delta\lambda_i \delta U_{iF} \tag{48}$$

with $\delta U_{iR} = -{K_T}^{-1} R_i$ (R_i is the difference between the internal load vector and the external one) and $\delta U_{iF} = {K_T}^{-1} F$.

With $\Delta U_{i+1} = \Delta U_i + \delta U_i$, $\Delta\lambda_{i+1} = \Delta\lambda_i + \delta\lambda_i$ and $D_i = \Delta {U_i}^T \Delta U_i + \Delta {\lambda_i}^2 \psi^2 F^T F - \Delta l^2 = 0$, the condition $D_{i+1} = 0$ leads to a quadratic equation in $\delta\lambda_i$. $\delta\lambda_i$ can then be used to compute δU_i and the (i+1)-th iteration can be completed.

However, two major problems occur at this stage of the procedure : the first one deals with the choice of root for the quadratic equation, and the other concerns the occurence of complex roots.

The solution to the first problem consists in finding the root that prevents from coming back on the continuation path. A good criterion is to take the root that gives the minimum angle between the difference $U_p - U_{p-1}$ (U_{p-1} and U_p are the two last converged increments) and ΔU_{i+1} at the current iteration.

Before addressing the second problem, it should be emphasized that prediction at the beginning of each increment plays a crucial role. The arc-length at the first iteration of each increment

depends on the arc-length of the previous converged increment through the relation :

$$\Delta l_{new} = \Delta l_{old} \frac{N_{opt}}{N_{old}} \tag{49}$$

where N_{opt} is the desired number of iterations to each converged increment, and N_{old} and Δl_{old} are the number of iterations and the arc-length used in the previous increment, respectively. Such good step control ensures relatively fast convergence.

Then :

$$|\Delta\lambda_1| = \frac{\Delta l}{\sqrt{\Delta U_1{}^{*T} \Delta U_1{}^* + \psi^2 F^T F}} \tag{50}$$

with the same sign as $(U_p - U_{p-1})^T \Delta U_1{}^*$ ($\Delta U_1{}^* = K_T{}^{-1} F$) for the procedure to stay in the sense it is currently advancing.

2.2.2 A new method for avoidance of complex roots The procedure has first to be reformulated to resolve this particular difficulty.

The out-of-balance loads may be resolved into a component $g_i F$ in the applied load direction and a component h_i orthogonal to F, with :

$$g_i = \frac{R_i{}^T F}{F^T F}, \; h_i = R_i - g_i F \tag{51}$$

δU_{iR} will be replaced by $\delta U_{ih} = -K_T{}^{-1} h_i$. The new incremental quantities will be obtained as :

$$\begin{aligned} \Delta U_{i+1} &= \Delta U_i + \delta U_{ih} + x_i \delta U_{iF} \\ \Delta\lambda_{i+1} &= \Delta\lambda_i + g_i + x_i \end{aligned} \tag{52}$$

The constraint equation then becomes quadratic in x_i.

The previous changes are purely formal and they do not prevent the quadratic equation to have complex roots. This decomposition only shows that the orthogonal component h_i of the residual R_i is mainly responsible for the occurence of complex roots.

Then, two corrective actions are possible. The first one consists in eliminating h_i directly by forcing :

$$\Delta U_{cr} = \Delta U_i + \delta U_{ih} \tag{53}$$

Once the internal force vector at the new displacement has been estimated, the incremental load factor can be computed, and then the new arc-length. To come back to the specified arc-length, a scaling factor will multiply ΔU_{cr} and $\Delta\lambda_{cr}$ to give ΔU_{i+1} and $\Delta\lambda_{i+1}$.

This simple method often leads to the divergence of the algorithm as a whole. A new and better idea would be to add a factor η_i in Eq.(52). It would then become :

$$\begin{aligned} \Delta U_{i+1} &= \Delta U_i + \eta_i \delta U_{ih} + x_i \delta U_{iF} \\ \Delta\lambda_{i+1} &= \Delta\lambda_i + g_i + x_i \end{aligned} \tag{54}$$

Unless the equation making the discriminant of the constraint equation in x_i to vanish gives complex roots η_i, which is fortunately rare, it is possible to find a good value of η_i, such that the constraint equation has no longer complex roots, and not too far from unity, in order to eliminate the most important part of the orthogonal residual as much as possible.

This new method seems to give satisfactory results in ensuring the same fast convergence as if there were no complex roots.

3 NUMERICAL EXAMPLES

Numerical examples are presented in this section in order to illustrate the robustness of both previous elastoplastic shell finite element model and solution procedure. Comparisons are presented with reference numerical results found in the literature.

3.1 Pinched elastoplastic cylinder

The first example consists in a short cylinder bounded by two rigid diaphragms at its ends and pinched by two concentrated forces at its middle section. The elastoplastic material response is governed by a linear isotropic hardening.

The cylinder is of length $l = 600.$, radius $R = 300.$ and relative thickness $h/R = 1/100$. The material properties are the same as in Brank *et al.* (1997) : Young modulus $E = 3.E3$, Poisson ratio $\nu = 0.3$, initial yield stress $\sigma_0 = 24.3$.

Simo and Kennedy (1992) have already considered this example, but with a stress-resultant elastoplastic shell model. Brank *et al.* (1997) have then found a snap-through behavior in the cylinder, which is not in accordance with the previous results. It divides the evolution of the cylinder deformation into two parts with two global stiffnesses which remain almost constant in each part.

The results of the present model are totally in accordance with the latter reference. This agreement, and especially the presence of a snap-through mechanism for these two models, can be explained by the similarity in the numerical integration scheme through the thickness of the shell.

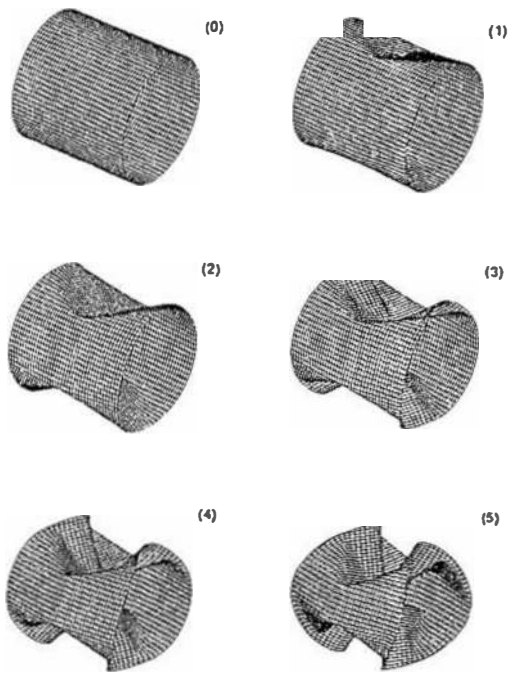

Figure 1. Pinched elastoplastic cylinder : deformed finite element mesh at various stages of loading

Deformed finite element meshes are presented for different load stages in Fig.(1). The pinching load is plotted against the radial displacement in Fig.(2).

3.2 Elastoplastic cylinder under axial compression

Many authors have performed experimental or numerical investigations about plastic buckling of axially compressed cylindrical shells. There are several types of response consisting in different plastic buckling modes depending on the boundary conditions of the cylinder (clamped, simply supported or free) and different ratios linking length and radius of the cylinder and especially radius and thickness.

For special values of the previous parameters, and especially for moderately thick and clamped shells, under displacement control, the axisymmetric mode (already encountered in elasticity) leads to a non-axisymmetric mode corresponding to a secondary bifurcation path, and leading itself to a "diamond" mode, directly encountered for thicker shells.

Goto and Zhang (1999) recently made a review of these transition modes and called them "elephant foot" modes. The present model, with an other plasticity approach, similarly show the occurence of such modes.

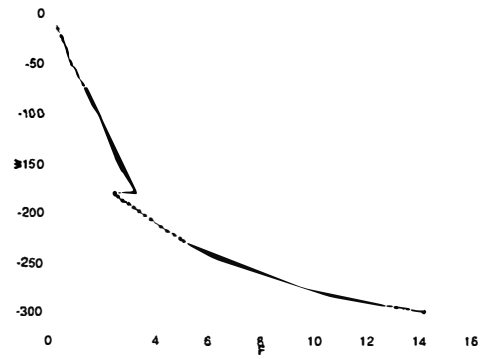

Figure 2. Pinched elastoplastic cylinder : displacement versus load curve

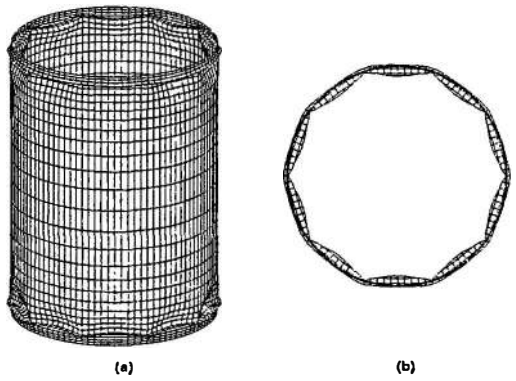

Figure 3. Elastoplastic cylinder under axial compression : "elephant foot" mode

The geometry is now defined by : length $l = 0.3$, radius $R = 0.1$ and relative thickness $h/R = 1/200$. The material properties are chosen so as to best reproduce Goto and Zhang's results (1999) : Young modulus $E = 2.1E11$, Poisson ratio $\nu = 0.3$, initial yield stress $\sigma_0 = 3.E8$. Besides, the non-linear hardening law is expressed as an exponential function of the equivalent plastic strain.

Two views of an "elephant foot" mode are depicted in Fig.(3).

CONCLUSION

A model for thin elastoplastic shells has been presented in this work including the von Mises yield criterion and a mixed

isotropic-kinematic hardening. The developed finite element allows finite rotations and large deformations. Numerical integration is employed over the shell thickness.

The solution procedure is based on a Newton-Raphson scheme and especially involves a new effective arc-length method for passing through limit points.

The proposed approach is also clearly adapted for non-linear applications such as buckling and post-buckling phenomena.

REFERENCES

BATHE K. J., *Finite element procedures.* Prentice-Hall, 1996.

BRANK B., PERIC D., ET DAMJANIC F. B., "On large deformations of thin elastoplastic shells : implementation of a finite rotation model for quadrilateral shell element", *International Journal for Numerical Methods in Engineering*, Vol. 40, pp. 689–726, 1997.

CRISFIELD M. A., *Non-linear finite element analysis of solids and structures.* John Wiley & Sons, 1991.

CURNIER A., *Méthodes numériques en mécanique des solides.* Presses polytechniques et universitaires romandes, 1993.

GERADIN M., "The finite element approach to kinematics and dynamics of flexible multibody systems", *Technical report, University of Liège, Belgium*, 1990.

GOTO Y. ET ZHANG C., "Plastic buckling transition modes in moderately thick cylindrical shells", *Journal of Engineering Mechanics*, Vol. 125, No. 4, 1999.

HELLWEG H. B. ET CRISFIELD M. A., "A new arc-length method for handling sharp snap-backs", *Computers and Structures*, Vol. 66, No. 5, pp. 705–709, 1998.

LAM W. F. ET MORLEY C. T., "Arc-length method for passing limit points in structural calculation", *Journal of Structural Engineering*, Vol. 118, No. 1, 1992.

NGUYEN Q. S., *Bifurcation and stability of dissipative systems.* International Centre for Mechanical Sciences, Springer-Verlag, 1993.

PETRYK H., "Plastic instability : criteria and computational approaches", *Archives of Computational Methods in Engineering*, Vol. 4, pp. 111–151, 1997.

POTIER-FERRY M., "Foundations of elastic postbuckling theory, in Buckling and Postbuckling", *Lectures Notes in Physics*, Vol. 288, pp. 1–82, 1986.

SIMO J. C. ET TAYLOR R. L., "A return mapping algorithm for plane stress elastoplasticity", *International Journal for Numerical Methods in Engineering*, Vol. 22, pp. 649–670, 1986.

SIMO J. C. ET KENNEDY J. G., "On a stress-resultant geometrically exact shell model. Part V. Non-linear plasticity : formulation and integration algorithms", *Computer Methods in Applied Mechanics and Engineering*, Vol. 96, pp. 133–171, 1992.